

Implanted neural electrodes cause chronic, local inflammation that is correlated with local neurodegeneration

This article has been downloaded from IOPscience. Please scroll down to see the full text article.

2009 J. Neural Eng. 6 056003

(<http://iopscience.iop.org/1741-2552/6/5/056003>)

[The Table of Contents](#) and [more related content](#) is available

Download details:

IP Address: 130.207.50.192

The article was downloaded on 02/04/2010 at 14:52

Please note that [terms and conditions apply](#).

Implanted neural electrodes cause chronic, local inflammation that is correlated with local neurodegeneration

George C McConnell¹, Howard D Rees^{2,3}, Allan I Levey^{2,3},
Claire-Anne Gutekunst⁴, Robert E Gross⁴ and Ravi V Bellamkonda¹

¹ Wallace H Coulter Department of Biomedical Engineering, Georgia Institute of Technology/Emory University, 313 Ferst Drive, Atlanta, GA 30332, USA

² The Center for Neurodegenerative Disease, Emory University, Atlanta, GA 30332, USA

³ Department of Neurology, Emory University, Atlanta, GA 30332, USA

⁴ Department of Neurosurgery, Emory University, Atlanta, GA 30332, USA

E-mail: ravi@gatech.edu

Received 17 April 2009

Accepted for publication 17 July 2009

Published 21 August 2009

Online at stacks.iop.org/JNE/6/056003

Abstract

Prosthetic devices that are controlled by intracortical electrodes recording one's 'thoughts' are a reality today, and no longer merely in the realm of science fiction. However, widespread clinical use of implanted electrodes is hampered by a lack of reliability in chronic recordings, independent of the type of electrodes used. One major hypothesis has been that astroglial scar electrically impedes the electrodes. However, there is a temporal discrepancy between stabilization of scar's electrical properties and recording failure with recording failure lagging by 1 month. In this study, we test a possible explanation for this discrepancy: the hypothesis that chronic inflammation, due to the persistent presence of the electrode, causes a local neurodegenerative state in the immediate vicinity of the electrode. Through modulation of chronic inflammation via stab wound, electrode geometry and age-matched control, we found that after 16 weeks, animals with an increased level of chronic inflammation were associated with increased neuronal and dendritic, but not axonal, loss. We observed increased neuronal and dendritic loss 16 weeks after implantation compared to 8 weeks after implantation, suggesting that the local neurodegenerative state is progressive. After 16 weeks, we observed axonal pathology in the form of hyperphosphorylation of the protein tau in the immediate vicinity of the microelectrodes (as observed in Alzheimer's disease and other tauopathies). The results of this study suggest that a local, late onset neurodegenerative disease-like state surrounds the chronic electrodes and is a potential cause for chronic recording failure. These results also inform strategies to enhance our capability to attain reliable long-term recordings from implantable electrodes in the CNS.

(Some figures in this article are in colour only in the electronic version)

1. Introduction

Prosthetic devices that are controlled by intracortical electrodes recording multiple single units are a reality today, and no longer merely in the realm of science fiction [1–7]. However, widespread clinical use of implanted electrodes is hampered by a lack of reliability in chronic recordings,

independent of the type of electrodes used. By recording reliability we mean the ability to predictably obtain a high percentage of electrodes with good quality single/multi units for several years after the implant. One major hypothesis in the field has been that astroglial scar, formed around implanted electrodes either due to insertion-associated injury, presence of a foreign material and/or due to mechanical mismatch

between the stiffness of the electrode and the brain, isolates the implanted electrodes from the brain, resulting in recording failure.

However, there are several reasons why the astroglial scar, per se, may not be the cause of recording signal degradation and unpredictability in obtaining long-term recordings. First, the impedance changes due to scar are not so dramatic that they should interfere with ability to record [8]. Second, chronic recording failure often occurs several weeks after a scar has developed and stabilized from an electrical perspective [9–12]. Therefore, the observation that it is not until several weeks after electrical impedance has stabilized that neural signals fade implies that the electrical properties of the scar are likely not the primary reason for recording failure/unreliability.

Previous studies have suggested that chronic inflammation surrounding the microelectrodes is persistent and is accompanied by neuronal cell death and loss of processes 4 weeks post-implantation [13, 14]. However, little is known about the state of target neurons at more chronic end points, nor whether or not degeneration of target neurons is correlated with chronic inflammation at the electrode interface. In this study, we investigated the tissue response to implant durations of 8 weeks and 16 weeks, long after the astroglial scar electrically stabilized [15, 16] and more in line with when researchers have reported that recording failure occurs. We hypothesized that chronic recordings fail due to a local neurodegenerative state developing in the vicinity of chronically implanted electrodes, and that this neurodegenerative state is characterized by neuronal loss, dendritic loss and axonal pathology in close proximity to the electrode surface, leading to recording signal loss/degradation due to the ‘unplugging’ of surviving neurons close to the electrode (<200 μm from the electrode surface) from their physiological networks. As a first step toward testing this hypothesis, we demonstrate that chronic, local inflammation due to the continuous presence of implanted electrodes is correlated with local neurodegeneration characterized by neuronal loss, dendritic loss and tauopathy.

2. Materials and methods

2.1. Surgical procedures for chronic implants

‘Michigan probes’ with four shanks were used in this study (NeuroNexus Technologies). Three end points after electrode implantation were investigated and were chosen based on the time course of astroglial scar development: 2 weeks, 8 weeks and 16 weeks. Rats were implanted with electrodes with a thickness of 15 μm , a length of 4 mm, a shank width of 60–100 μm and tip spacing of 200 μm (abbreviated 4 mm_200). As a control for the acute injury due to electrode insertion, an additional group of six rats was inserted with electrodes and retrieved 2 min after insertion (abbreviated S.W. for stab wound), then was sacrificed 16 weeks later. In a previous study we found that decreased shank spacing resulted in increased astrogliosis after 4 weeks [17]. Therefore, an additional group of animals was implanted with an electrode design of closer inter-shank spacing to study the influence of increased chronic

Table 1. Experimental design: animal numbers for conditions.

Duration (weeks)	4 mm_200			
	4 mm_200	3 mm_125	(stab wound)	No implant
2	6	0	0	0
8	5	0	0	0
16	6	6	6	2

inflammation on nearby neurons. Six rats were implanted with electrodes with a thickness of 15 μm , a length of 3 mm, a shank width of 30–100 μm and a tip spacing of 125 μm (abbreviated 3 mm_125) at only the 16 week end point (See table 1 for experimental design.).

Adult male Sprague-Dawley rats (275–299 grams) were anesthetized prior to surgery using a mixture of 5% isoflurane and 1 L min^{-1} O_2 . Each rat was then positioned into a stereotaxic frame (Kopf) where anesthesia was maintained to effect (\sim 1–3% isoflurane and 0.3 l min^{-1} O_2) during surgery by monitoring the rat’s breathing. The rat’s head was shaven over the incision area and the skin was disinfected with isopropyl alcohol and chlorohexaderm using a slight scrubbing motion before making the incision. Ophthalmic ointment was applied to the eyes to prevent drying. A midline incision was made along the scalp, the skin retracted and the periosteum cleared to expose the bregma. A dental drill was used to create a 3.2 mm hole at +0.2 mm anterior and +3.0 mm lateral to the bregma with a custom trephine (24 tooth \times 3 mm O.D.) fabricated from stainless steel tubing (Small Parts). In order to minimize iatrogenic damage, room temperature saline was applied liberally to the spinning drill bit at the bone interface. The bone plug was carefully removed and the dura was gently pierced and retracted using a 28 gauge needle with the tip bent at a 45° angle. The bond-pad region of the microelectrode was grasped with Teflon-coated microforceps and the penetrating shanks were inserted stereotaxically through the pia mater into the cortex. Care was taken to minimize bleeding by avoiding insertion through large surface blood vessels. The electrode was inserted to the point where only the bond-pad region was visible outside the cortical surface. After the insertion, the bond-pad region of the electrode and the craniotomy were covered with 1% SeaKem Agarose (Cambrex) gel in phosphate buffered saline (PBS). A craniotomy of identical diameter was made over the contralateral location (+0.2 mm anterior to the Bregma and –3.0 mm lateral to the midline suture) where an additional electrode, of identical design to that implanted in the contralateral hemisphere, was inserted and protected with agarose the same way as described above. The craniotomies were further sealed and protected using dental acrylic anchored to the skull with bone screws (Plastics One, Inc.). The skin was closed with wound clips and the rats were monitored until recovery from anesthesia. To minimize variability associated with the surgery, all implants were performed by the same surgeon. All procedures were approved by Georgia Tech Institutional Animal Care and Use Committee.

2.2. Brain tissue preparation for immunohistochemistry

After 2 weeks, 8 weeks or 16 weeks, each animal was anesthetized with a mixture of ketamine (45.65 mg kg^{-1}),

Table 2. List of primary antibodies.

Primary	Host	Isotype	Dilution	Vendor	Antigen	Cell specificity
CD68 (ED-1)	Ms	IgG1	1:1000	Serotec	Lysosomal glycoprotein	Activated microglia/macrophages
GFAP	Rb	IgG	1:2000	DAKO	Glial fibrillary acidic protein	Astrocytes
NeuN	Ms	IgG1	1:500	DAKO	Neuronal nuclei	Neurons
MAP-2	Ms	IgG1	1:1000	Chemicon	Microtubule-associated protein	Neurons
NF-200	Rb	IgG	1:1000	Sigma	Heavy neurofilament polypeptide	Neurons
Tau-1	Ms	IgG2a	1:200	Chemicon	Microtubule-associated protein	Neurons
pT231	Ms	IgG1	1:2000	Chemicon	PhosphoThreonine 231	Neurons

xylozine (9.13 mg kg⁻¹) and acepromazine (1.52 mg kg⁻¹), then transcardially perfused with PBS prewash followed by 4% paraformaldehyde in PBS. The brains were removed and postfixed overnight (4 °C). Following the retrieval of the electrodes, rat brains were placed into 30% sucrose (4 °C) until they sunk to the bottom. A tissue dye was then carefully applied to the left-posterior hemisphere to later identify the orientation of the brain sections and align images with the same electrode orientation. The brains were then cryoprotected with optimal cutting temperature (O.C.T.) compound (Tissue-Tek). The horizontal tissue sections were cut to a final depth of ~2 mm from the surface of the cortex for all brains. The serial sections were cut 30 µm in thickness with the exception of every 13th section, which was cut 14 µm in thickness. The 14 µm sections were mounted directly to a glass slide and stained with hematoxylin and eosin (H&E) using a Leica Autostainer XL, while the 30 µm sections were serially stored in two six-well plates at 4 °C in PBS with 0.01% sodium azide to minimize bacterial contamination.

2.3. Immunohistochemistry

To study brain tissue response, sections taken from all brains were stained simultaneously for the antibody of interest. Sections from adjacent wells, with five sections per well, were used to stain for ED-1, MAP-2 and double-stain for GFAP/NeuN, and NF-200/tau-1, respectively. These stains were used to visualize the presence of activated microglia/macrophages (ED-1), astrocytes (GFAP), neuronal nuclei (NeuN), dendrites (MAP-2) and axons (NF-200 and tau-1) (table 2). The five sections per well ranged from ~200 µm to ~2 mm below the surface of the cortex and were spaced at uniform intervals of 374 µm. The sections were blocked in 4% normal goat serum (GIBCO) with PBS containing 0.5% Triton X-100 (Sigma) for 1 h at room temperature. The sections were then immediately incubated overnight at 4 °C with primary antibody prepared in blocking solution. Primary antibodies used are shown in table 2. After washing in 0.5% triton in PBS, the sections were incubated in secondary antibodies for 1 h at room temperature. Secondary antibodies were diluted at a ratio of 1:220 in 0.5% triton in PBS, and included goat anti-rabbit IgG (H + L) Alexa 488 (molecular probes) and goat anti-mouse IgG1 Alexa 594 (molecular probes). All sections were counterstained by incubation with the nuclear dye DAPI (molecular probes) that labels all cell nuclei. An additional cortical section from each rat brain was used to control for non-specific secondary antibody labeling, by omitting the

primary incubation step (primary control). The tissue sections were mounted on glass microscope slides with fluoromount-G (Southern Biotechnology Associates).

For hyperphosphorylated tau staining, two additional rats were implanted with four-shank silicon microelectrode arrays (4 mm_200 design) and perfused 16 weeks later using 4% paraformaldehyde + 0.1% glutaraldehyde. Brains were then postfixed 1 h in the same solution and sectioned using a vibratome (thickness = 50 µm). Brain tissue from a Parkinson's disease (PD) patient was also studied. The patient was a 63 year old man with a 13 year old history of intractable PD. Ten years after symptom onset the patient received microelectrode-guided implantation of a deep brain stimulator in the left subthalamic nucleus. Three years later a deep brain stimulator was placed in the right subthalamic nucleus. The patient died 5 months post-implantation. At autopsy, the entire brain was placed in cold 4% paraformaldehyde for 8–15 h, then removed, blocked and returned to fresh fixative for a total of 24–36 h of fixation. Tissue blocks were then rinsed in 0.1 M sodium phosphate buffer (PB), pH 7.3, and were placed in cold 20% glycerol/2% DMSO solution or 30% sucrose/30% ethylene glycol. Tissue blocks were further dissected and the serial sections were cut at 50 µm using a freezing microtome. The cut sections were stored in cryoprotectant at –20 °C for subsequent analysis. After five rinses in PBS, the sections were incubated for 10 min in 3% hydrogen peroxide. The sections were rinsed, and blocked for 1 h at 4 °C in blocking solution containing 8% horse serum, avidin (10 µg ml⁻¹) and 0.1% Triton-X. The sections were then incubated with pT231 (see table 2), AT8 (Pierce; 1 µg ml⁻¹), or Alz50 (diluted 1:100) in solution with 2% horse serum and biotin (50 µg ml⁻¹). Next, the sections were incubated with biotinylated donkey anti-mouse secondary (Jackson immunochemicals; dilution 1:200 for 1 h at 4 °C, and then visualized using a VECTASTAIN Elite ABC kit (Vector Laboratories). Horseradish peroxidase was visualized using DAB as the substrate.

2.4. Fluoro-Jade C staining

The sections were stained using Fluoro-Jade C, a sensitive marker for degenerating neuronal cell bodies and processes, as previously described [18]. Briefly, the sections were mounted onto gelatinized slides and dried overnight at room temperature. The slides were immersed in 100% EtOH for 3 min, followed by 70% EtOH for 1 min, and rinsed with distilled water. The slides were placed in 0.06% KMnO₄ on a shaker plate for 15 min. After rinsing in distilled water for

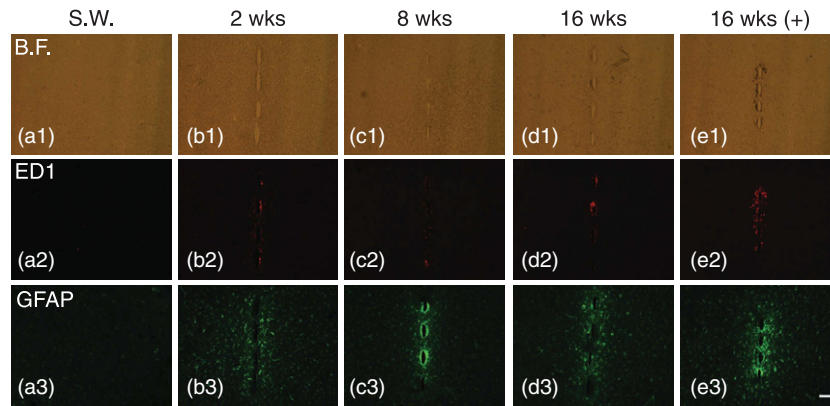


Figure 1. Representative bright field (B.F.) (a1)–(e1), ED-1 (a2)–(e2) and GFAP (a3)–(e3) stained images from all conditions. Horizontal sections contain the four electrode tracks in the center of each image. Stab wound (S.W.). The scale bar is 100 μm .

1 min, the slides were stained in a solution of 0.001% Fluoro-Jade C dissolved in a 0.1% acetic acid vehicle. The sections were rinsed three times in distilled water, then dried at room temperature, cleared and coverslipped.

2.5. Quantitative analysis of histological images

Quantitative analysis was obtained from 12 implant sites (two implants per animal) for each condition with the exception of the 8 weeks condition which contained 10 implant sites. Fluorescent and bright field images were acquired using a microfire digital camera and a Zeiss Axioskop2 Plus upright microscope with a 10 \times objective, with the electrode sites centered in the camera field (figures 1 and 4). Four sections approximately 200 μm , 600 μm , 1000 μm and 1400 μm below the brain surface were imaged for quantification to investigate the response at different depths in the cortical column. All tissue sections were imaged in a single session to minimize variability. The exposure time was consistent within each marker and was set below saturation of the digital camera. Fluorescent intensity as a function of distance from the electrode–tissue interface was calculated for GFAP, ED-1, MAP-2, tau-1, NF-200 and Fluoro-Jade C stained sections using MATLAB (with Image Processing Toolbox, Mathworks), as previously described [17]. Briefly, the images were first rotated such that the four insertion sites were aligned vertically. An ellipse was computed from five or more user-specified points around each of the four insertion sites using the bright field image to delineate the electrode–tissue interface and the location of the ellipses was then saved to file. The saved ellipse points were then used in the corresponding immunostained images to segment rectangular regions from the middle of each ellipse to a distance of 500 μm away for both the left and right sides. The intensity values of each of the boxed regions were then averaged along the y -axis to create two mean intensity profiles for each insertion site. The mean of the eight line profiles was then computed. For normalization, the average intensity from 400–500 μm in each image was subtracted from the intensity profile 0–500 μm . The integral of the mean intensity profile at six different distance increments along the electrode (0–50 μm , 50–100 μm , 0–100 μm , 100–200 μm , 200–300 μm and 300–500 μm) was also calculated

for each image. NeuN images were segmented using a marker-based watershed algorithm.

2.6. Statistical analysis

All statistical inferences were made between differing time points using one-way standard analysis of variance. When we found a significant difference between groups, we performed the Tukey's honest significant difference (HSD) *post-hoc* test to identify pairwise differences. For all tests, $p < 0.05$ was considered significant.

3. Results

3.1. Evidence for local, persistent inflammation

3.1.1. Activated microglia (ED-1). Activated microglia form a front line of defense, and their presence was primarily at the electrode interface. Predominantly, they were found within the first 25 μm away from the electrode (figure 2(a)). Few activated microglia were observed after 2 weeks. After 8 weeks, the numbers were slightly larger, and had decreased again after 16 weeks (figure 2(b)). After 16 weeks, the 125 μm spaced electrode design showed the greatest number of activated microglia compared to any condition. In the case of stab wound, no ED-1 (+) signal was observed.

3.1.2. Astrocytes (GFAP). As expected from previous studies, GFAP expression was increased in the tissue surrounding the microelectrodes [19, 20]. The characteristics of the GFAP expression differed with the distance from the electrode at the three different end points (2, 8 and 16 weeks) (figures 1 and 2(c)). After 2 weeks, the peak of the intensity curve was at ~ 50 μm away from the electrode. After 8 weeks, the peak in the GFAP expression was even closer to the electrode. After 16 weeks, the expression levels of GFAP were next to the electrode, but were more distant from the electrode compared to the 8 week time point and had decreased in intensity. Any indication of increased GFAP relative to background surrounding the electrode tracks was not observed in the case of the stab wound. GFAP levels for the 125 μm , 16 week (+) control, electrode design had a similar profile to

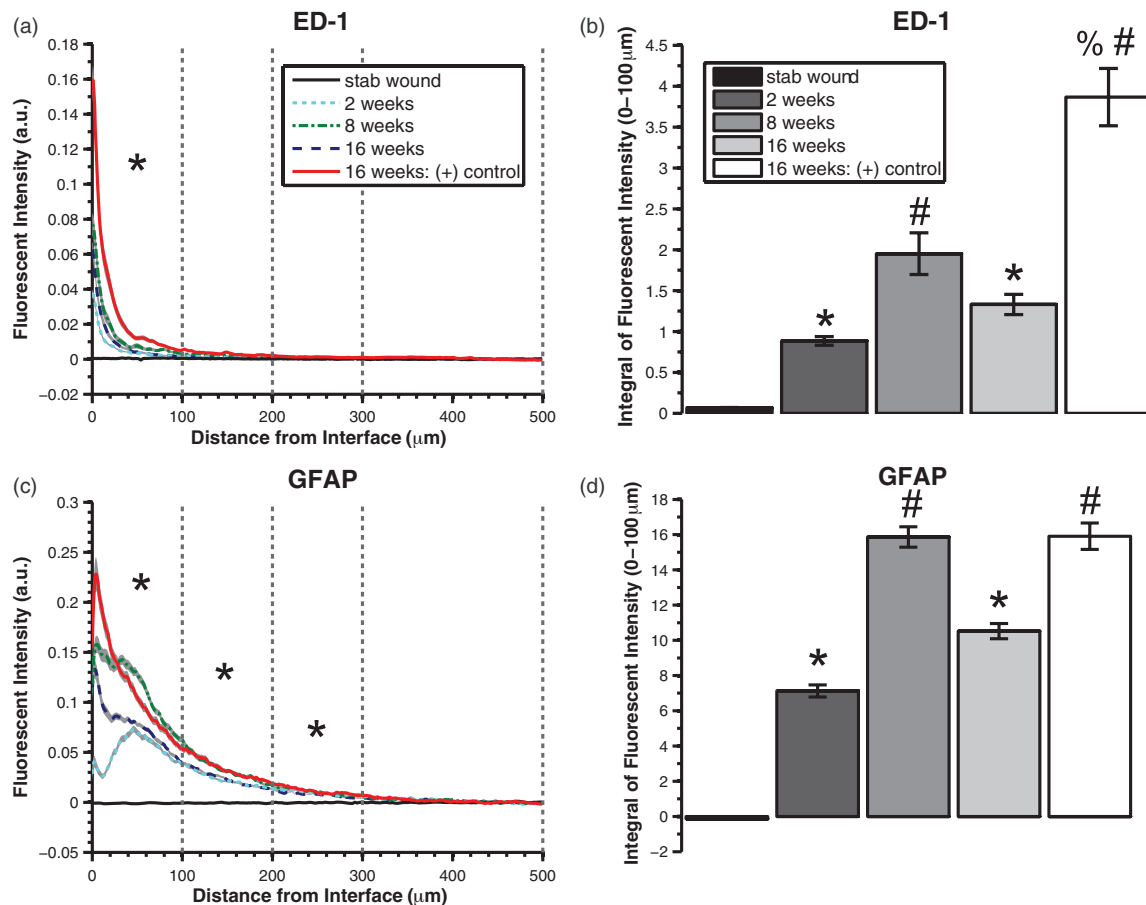


Figure 2. Quantified ED-1 expression (for activated microglia) and GFAP expression (for astrocytes). Results are the mean of the four most superficial sections and are spaced 374 μm through the cortical column. In (a) and (c) the mean ± SEM (SEM indicated by gray filled area surrounding lines) are shown. Bar graphs in (b) and (d) represent mean ± SEM. * represents significantly higher than stab wound condition ($p < 0.05$). # represents significantly higher than 8 week condition (and stab wound) ($p < 0.05$). (a) ED-1 fluorescent intensity as a function of distance from the electrode. ED-1(+) microglia are located primarily within the first 50 μm away from the electrode. (b) Integral of ED-1 fluorescent intensity 0–100 μm from the electrode. No ED-1 (+) signal is observed 16 weeks after stab wound injury. For groups in which the electrode remained in the brain for 16 weeks, the 125 μm spaced electrode design had significantly more ED-1 (+) signal, compared to the 200 μm spaced electrode design ($p < 0.05$). (c) GFAP fluorescent intensity as a function of distance from the electrode. (d) Integral of GFAP fluorescent intensity 0–100 μm from the electrode.

that of the 8 week 200 μm spaced electrode design, both being significantly higher than the 16 week condition (figure 2(d)).

3.1.3. Hemosiderin-laden macrophages. Hemosiderin is an iron-binding molecule in the blood, closely related to wüstite, an Fe²⁺ iron oxide. The presence of hemosiderin indicates that the lesion was hemorrhagic and has been speculated to be a byproduct of oxidative stress [21]. Since oxidative stress has been shown to lead to neurodegeneration [22, 23], we quantified the presence of hemosiderin-laden macrophages next to the electrode. The characteristic granular, olive brown appearance of hemosiderin-laden macrophages under bright field was used to identify the cells for counting (figures 3(a)–(c)). The deposits were co-localized with ED-1 staining (figure 1). Quantified hemosiderin-laden macrophages are shown in figure 3(d). Hemosiderin-laden macrophages were only present in three conditions: 8 weeks, 16 weeks and 16 weeks (+) control. These three conditions showed variability in the number of implants surrounded by hemosiderin-

laden macrophages (8 weeks: 3/12 implants, 16 weeks: 8/12 implants, 16 weeks (+) control: 11/12 implants). The 16 weeks (+) control condition contained significantly greater numbers of hemosiderin-laden macrophages compared to the other conditions (figure 3(d)).

3.2. Evidence for local, late onset neurodegeneration

In this section we discuss markers of neuronal health, first at the anatomical level and then at the molecular level.

3.2.1. Anatomical markers of neurodegeneration: neuronal viability (NeuN, Fluoro-Jade C). Neuronal loss was evident for all conditions within the first 100 μm away from the electrode with the exception of the stab wound condition (figure 6(a)). After 16 weeks, neuronal loss had significantly increased compared to 8 weeks p.i. up to 300 μm from the electrode surface. Comparing NeuN loss between the two electrode designs after 16 weeks, there was significantly

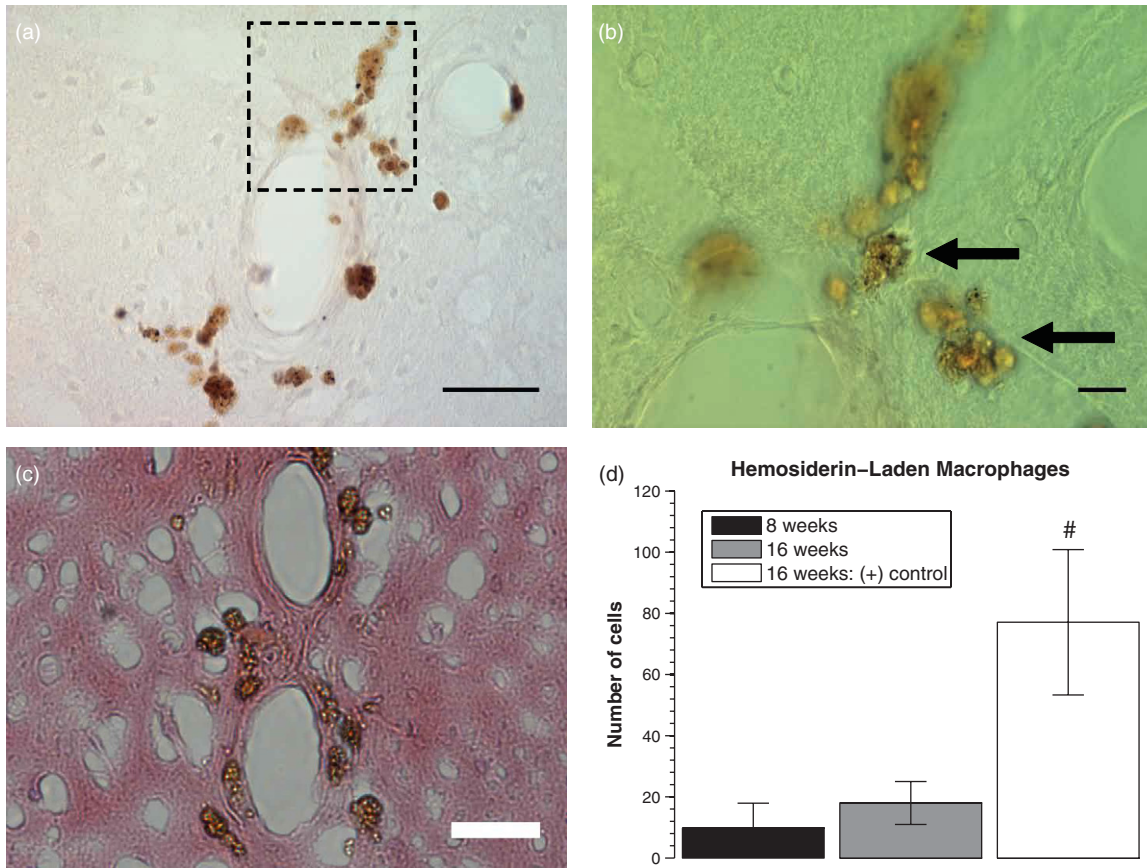


Figure 3. (a) Representative bright field image 16 weeks post-implantation showing hemosiderin-laden macrophages. The scale bar is 50 μm . (b) Boxed region in (a) at higher magnification. Arrows point to granular dark brown structures indicative of hemosiderin-laden macrophages. The scale bar is 10 μm . (c) Hematoxylin and eosin-stained section 8 weeks p.i. showing golden-brown hemosiderin granules. The scale bar is 50 μm . (d) Quantified hemosiderin-laden macrophages. Bar represents mean \pm SEM. # indicates significantly greater than 8 week and 16 week conditions ($p < 0.05$).

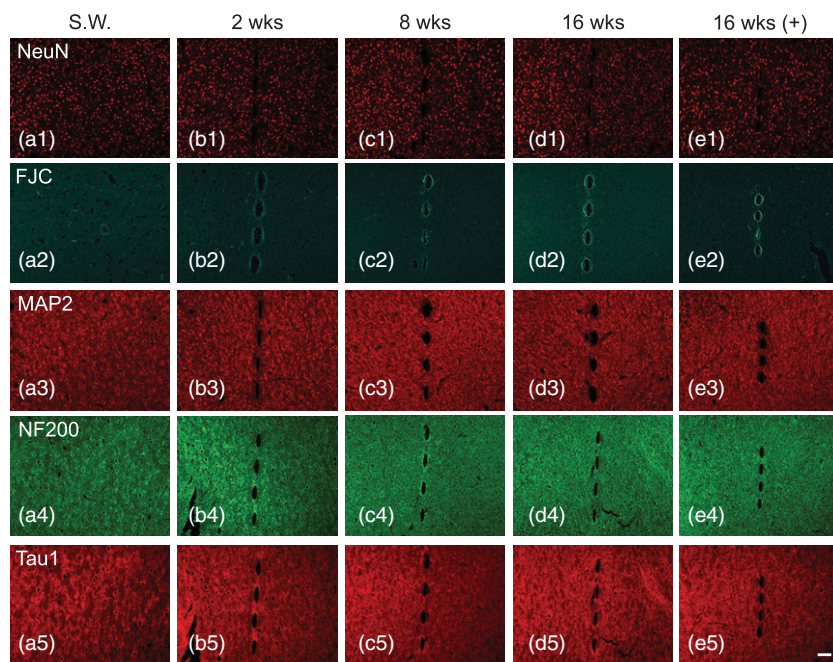


Figure 4. Representative NeuN (a1)–(e1), Fluoro-Jade C (a2)–(e2), MAP-2 (a3)–(e3), NF200 (a4)–(e4) and tau-1 (a5)–(e5) staining from all conditions. Horizontal sections contain the four electrode tracks in the center of each image. Stab wound (S.W.). The scale bar is 100 μm .

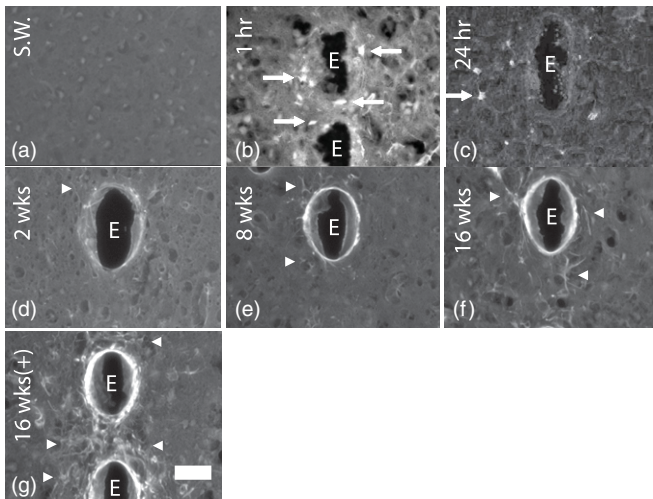


Figure 5. Neurodegeneration acutely versus chronically is fundamentally different. Fluoro-Jade C (for degenerating/dying neurons) stained neuronal death in the immediate vicinity after 1 h and 24 h (b) and (c). Arrows indicate degenerating cell bodies. After 2 weeks, degeneration was observed primarily in neuronal processes, with relatively few cell bodies stained (d)–(g). The greatest number of Fluoro-Jade C positive processes were observed surrounding the 3 mm₁₂₅ electrode tracks 16 weeks post-implantation (g). Arrow heads indicate degenerating processes. ‘E’ indicates electrode track. Stab wound (S.W.). The scale bar is 50 μm .

more loss in the case of the 3 mm₁₂₅ design compared to the 4 mm₂₀₀ design over the 0–100 μm and 200–300 μm intervals. Fluoro-Jade C staining was confined to processes (figures 4(c2)–(e2)). Fluoro-Jade C staining of similar implants 1 h and 24 h post-implantation showed staining of neuronal bodies, however, there was no evidence of apoptosis or necrosis for the 2, 8 and 16 week end points (figure 5). Fluoro-Jade C intensity in the first 100 μm was significantly higher after 16 weeks compared to 8 weeks (figure 6(c)).

3.2.2. Anatomical markers of neurodegeneration: dendrites (MAP-2). While the Fluoro-Jade C stain suggested neuronal processes were dying back near the electrode, it was unclear from these data whether the loss of processes was occurring due to dendrites and/or axons dying back. To further explore where this degeneration occurs, we used specific immunohistochemical stains for dendrites and axons. To investigate dendritic arborization surrounding the electrode, MAP-2 was fluorescently labeled, while NF-200 and tau-1 were used to investigate axonal arborization.

No loss in MAP-2 expression was observed in the case of the stab wound (figure 6(d)). For the other conditions MAP-2 staining intensity generally followed an inverse relationship with ED-1 expression (figure 6(d)). The 3 mm₁₂₅ electrode design had significantly less MAP-2 signal, compared to the 4 mm₂₀₀ electrode design in the first 100 μm from the electrode (figure 6(e)). Dendritic loss was most prominent at deeper depths of the cortical column, at depths of ~ 1000 μm and ~ 1400 μm (figure 7(d)).

3.2.3. Anatomical markers of neurodegeneration: axons (tau-1, NF-200). Unlike MAP-2, no differences were observed between conditions for the axonal markers tau-1 and NF-200.

3.2.4. Molecular markers of neurodegeneration: phospho-tau (pT231). A characteristic feature of many neurodegenerative diseases is axonal pathology manifested by hyperphosphorylation of protein tau (see table 1 of [24] for a list of neurodegenerative tauopathies). Given the association between oxidative stress and hyperphosphorylated tau in neurodegenerative diseases such as Alzheimer’s disease (AD), several markers for hyperphosphorylated tau were used. Tau protein, predominately located in axons, contains at least 30 epitopes which become abnormally phosphorylated in tauopathies like AD. There was no positive staining for Alz50 or AT8 (data not shown). PT231 staining was present only next to the electrode track, with negative controls showing an absence of staining. Within the first 50 μm from the electrode punctate staining was observed within neuron somas. Out to a distance of 700 μm from the electrode pT231 (+) dystrophic neurites and neuropil threads were observed, closely resembling those observed in an AD diseased human tissue section stained simultaneously (figure 8).

While deep brain stimulation (DBS) electrodes are mainly stimulatory, they are an example of a chronically implanted electrode in humans. Human brain tissue was obtained from a patient implanted with a DBS electrode, that had remained for 5 months. pT231 is upregulated in close proximity to the electrode (figure 9).

4. Discussion

While neuronal viability is a necessary condition for recordings, it is not sufficient. Not only must neurons be alive, they must also have normal network connectivity enabled by ‘normal’ dendritic and axonal trees, and functional cell bodies. In this study, we investigated neurodegeneration surrounding chronically implanted electrodes at 2 weeks, 8 weeks and 16 weeks after implantation. We varied the degree of chronic inflammation at the 16 week time point to test the hypothesis that chronic inflammation associated with the presence of the electrode is correlated with a neurodegenerative state. These data show that higher levels of activated microglia and reactive astrocytes are correlated with increased neuronal loss, dendritic loss and tauopathy surrounding the electrodes. These data support an intriguing hypothesis for the inconsistency commonly observed with chronic neural recordings: that the glial scar causes recording failure indirectly through local neurodegeneration.

Edell *et al* reported a ‘kill zone’ a distance of 10 μm away from the electrode [25]. Biran *et al* reported neuronal death surrounding electrodes at chronic time points (2 and 4 weeks) [13]. This paper also showed loss in neurofilament-160 within the first 100 μm from the electrode. The authors speculated that neurotoxic factors released by microglia best explain the neuronal loss. Our data show a progressive loss in number of neurons at chronic end points (increased loss at 16 weeks compared to 8 weeks). Furthermore, after 16 weeks there was

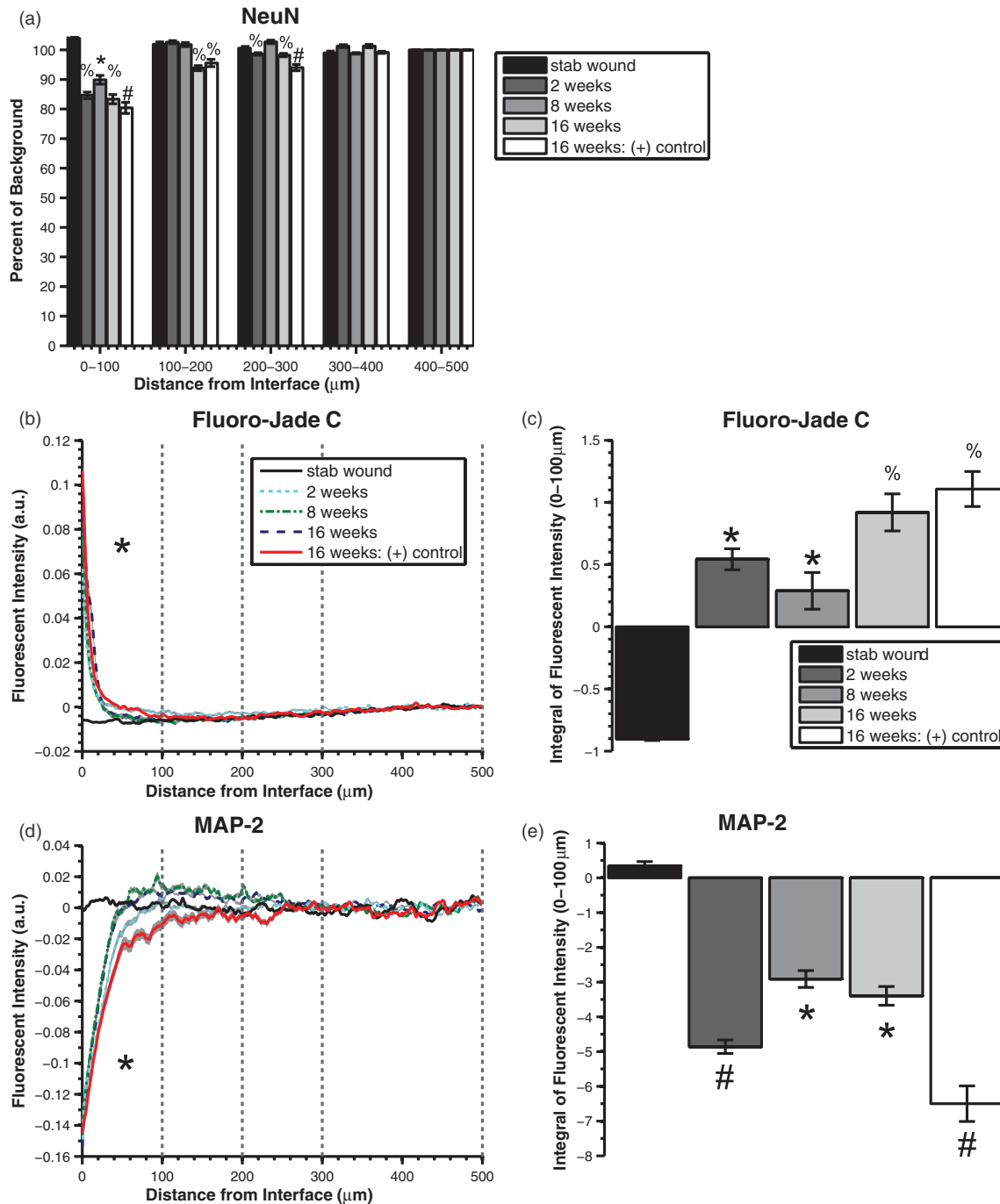


Figure 6. Quantified NeuN expression (for neuronal nuclei), Fluoro-Jade C (for degenerating/dying neurons) and MAP-2 (for dendrites). Results are the mean of the four most superficial sections and are spaced 374 μm through the cortical column. In (b) and (d) the mean ± SEM (SEM indicated by gray filled area surrounding lines) are shown. Bar graphs in (a), (c) and (e) represent mean ± SEM. * represents significantly higher than stab wound condition ($p < 0.05$). % indicates significantly greater than 8 week condition (and stab wound) ($p < 0.05$). # indicates significantly greater than 16 week condition (and stab wound and 8 weeks) ($p < 0.05$). (a) The number of NeuN (+) cells, represented as percent of cells 400–500 μm. (b) Fluoro-Jade C fluorescent intensity as a function of distance from the electrode. (c) Integral of Fluoro-Jade C fluorescent intensity 0–100 μm from the electrode. (d) MAP-2 fluorescent intensity as a function of distance from the electrode. (e) Integral of MAP-2 fluorescent intensity 0–100 μm from the electrode. Note: negative intensity denotes loss relative to background intensity.

greater neuronal loss in the case of the 3 mm₁₂₅ electrode design, associated with more inflammation, than in the case of the 4 mm₂₀₀ electrode design. The NeuN loss we observed was >20% less than that reported by Biran *et al*. This may be explained by our use of an untethered model compared to a

tethered model used by Biran *et al*, known to result in a larger inflammatory response [14].

To further study axonal and dendritic degeneration along with neuronal viability, we used Fluoro-Jade C staining, a useful marker for neurodegeneration [26–29]. Compared to its

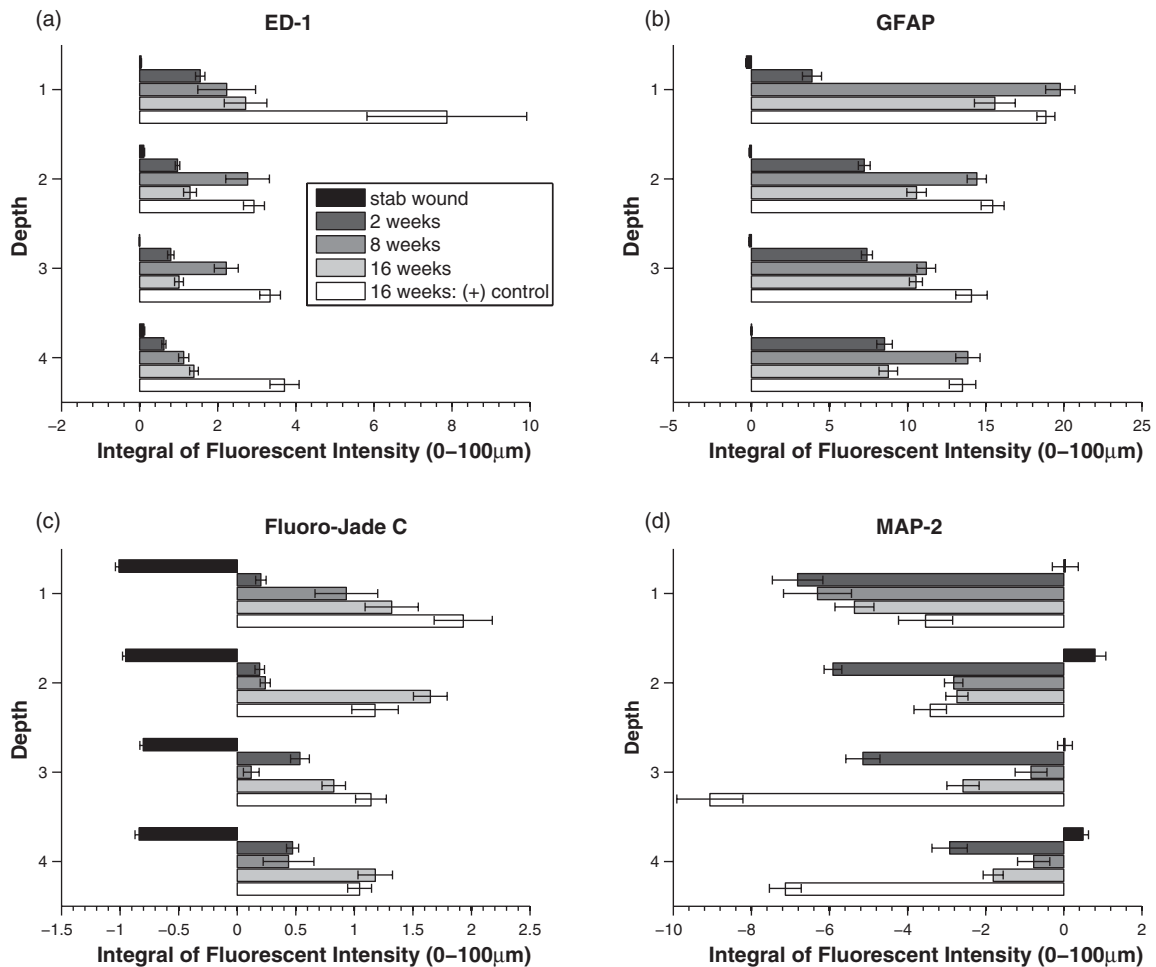


Figure 7. Quantified fluorescent intensity 0–100 μm from the electrode for (a) ED-1, (b) GFAP, (c) Fluoro-Jade C and (d) MAP-2 for sections at the four different depths studied. On the y-axis, tissue section 1 is $\sim 200 \mu\text{m}$ below the cortex, tissue section 2 is $\sim 600 \mu\text{m}$, tissue section 3 is $\sim 1000 \mu\text{m}$ and tissue section 4 is $\sim 1400 \mu\text{m}$.

predecessors, Fluoro-Jade B and Fluoro-Jade, Fluoro-Jade C is brighter and stains degenerating neuronal processes in addition to the soma. We hypothesized that axonal and dendritic degeneration would accompany neuronal death. The staining results revealed an early degeneration of neurons within 50 μm of the electrode at 1 h and 24 h post-implantation, but at 8 and 16 weeks post-implantation the marker revealed that degeneration is largely found in neuronal processes rather than in cell bodies. These data are consistent with a feature of neurodegenerative disease, that degeneration begins at the tip of the processes and works back toward the soma. Using immunohistochemistry, we further specifically labeled both dendrites (MAP-2) and axons (NF-200/tau-1). We observed significant loss from 8 weeks to 16 weeks in dendrites, but no significant difference in axonal markers. Dendritic loss was most striking at deeper depths of the cortical column (figure 10). One potential source for the loss is the difference in thickness of the electrodes from the bond-pad to the tip. Since the electrode thickness decreases from the bond-pad to the tip, this would not explain the observed increase in dendritic loss at deeper cortical layers. However, the increased size of the electrode may contribute to the increased glial markers in the more superficial layers (figures 7(a) and (b)). One possibility

is that neurons at deeper cortical depths are more susceptible to neurodegeneration than neurons at superficial depths. Since the tips of the electrodes are below the cortex, it is unlikely that the effects are due to micromotion. Regardless of the cause of the observed differences between depths, dendritic loss would be expected to have significant impact on processing of synaptic input and thus neural recordings.

No significant differences in NF-200/tau-1 staining suggests that axons were spared, or may indicate axonal sprouting. We further investigated the axonal state by looking for evidence of tau pathology. Positive staining was found for the marker pT231 [30], but not AT8 or Alz50. It is well known that there is a temporal sequence of phosphorylation of tau, with certain residues of the protein phosphorylated earlier than others. pT231 is one of the earliest sites of the tau protein to be phosphorylated [31]. T231 phosphorylation, occurring primarily in pre-tangles, precedes AT8, which occurs primarily in late stage extra-neuronal tangles [31]. It has also been shown that pT231 precedes Alz50 [32], and is therefore considered an earlier marker for tau tangles [33]. Therefore, our observation of pT231 positive signal with an absence of AT8 and Alz50 positive signal suggests that the tau pathology present in the surrounding microelectrodes in this study after 16 weeks is in

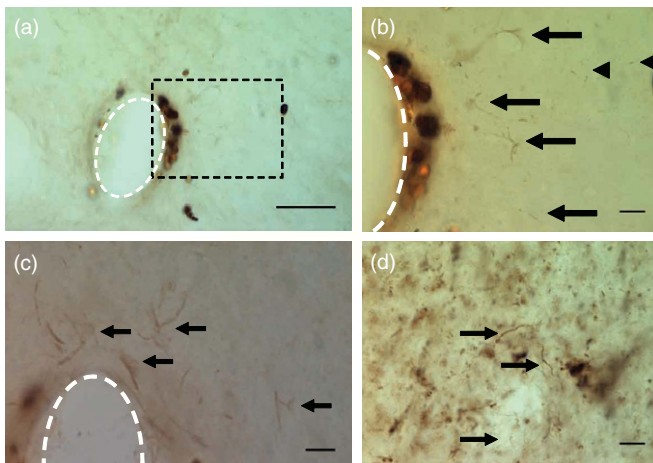


Figure 8. Hyperphosphorylated tau surrounding chronically implanted microelectrodes 16 weeks post-implant. (a)–(c) Representative images of pT231 immunostained pretangles. (b) Boxed region in (a) at higher magnification. Note the increased presence of pT231 staining near non-specifically stained hemosiderin-laden macrophages. (c) Additional example from another implant showing the pT231 positive signal surrounding the electrode. Arrows indicate labeled diffuse granular pretangles and arrow heads indicate rodlike dystrophic neurites. (d) Positive control—human Alzheimer's case sections contained stained processes similar to those seen around electrodes. The scale bar is 50 μm (a) and 10 μm (b)–(d).

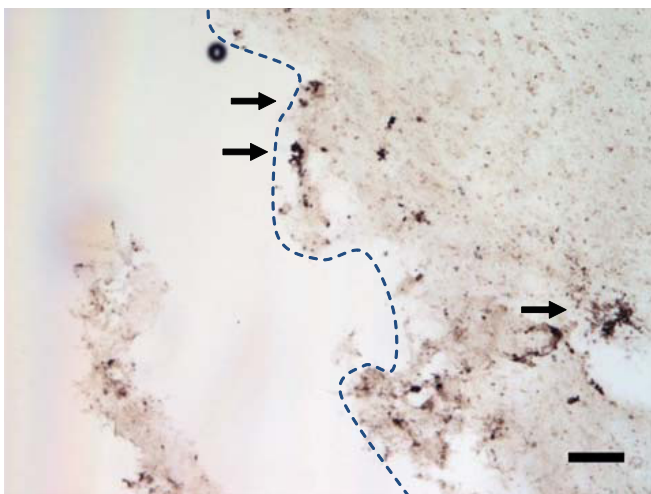


Figure 9. Hyperphosphorylated tau surrounding the chronically implanted electrodes in a human PD patient 5 months post-implant. Tissue adjacent to the electrode track showed upregulated expression of pT231, an abnormally hyperphosphorylated site on the tau protein. Arrows indicate regions of high pT231 expression. The scale bar is 100 μm .

the early stages of tau pathology. This is not to say, however, that there would not be functional consequences to pT231 alone. pT231 plays an important functional role in synaptic health [34, 35]. While paired helical filaments (PHFs), which are derived from hyperphosphorylation [36], are not apparent around electrodes after 16 weeks, pT231 precedes PHFs [37] and further studies are needed to investigate whether PHFs form > 16 weeks.

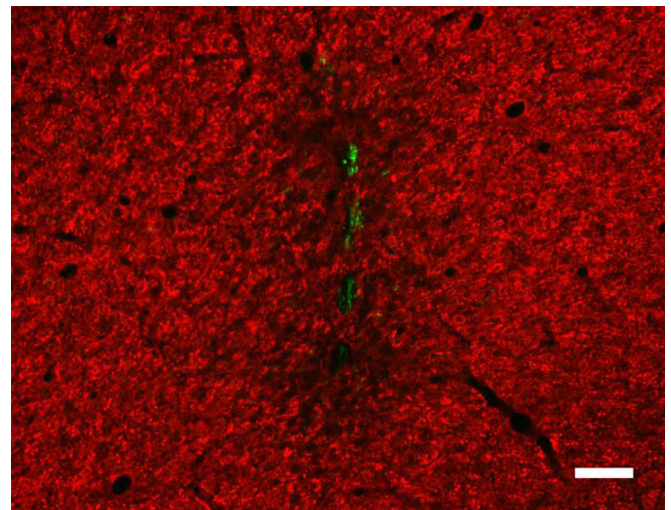


Figure 10. Merged Map-2 and ED-1 staining from consecutive tissue sections. Tissue sections are from 16 week (+) control condition at depth ~ 1 mm below the cortical surface. The scale bar is 100 μm .

The relationship between microglia and neurodegeneration has been an important topic of study in the neurodegenerative disease literature [22, 23, 38]. In one study, a single systemic injection of LPS caused chronic inflammation and progressive loss of dopaminergic neurons in the substantia nigra [39]. Other studies have investigated the relationship between inflammation and tau hyperphosphorylation, with oxidative stress reported to cause tau pathology [40, 41]. Kitazawa *et al* showed that inflammation induced by LPS exacerbates tau pathology [42]. Microglial activation has been shown to precede tau tangles in a P301S tauopathy mouse model and can be diminished by NSAIDs, suggesting a causative role by inflammation in the formation of tau tangles [43]. These studies are consistent with the rat and human pT231 staining from this study, where phospho-tau expression declines gradually as a function of distance from the surface of the electrode.

Hemosiderin-laden macrophages present suggest hemorrhaging of microvasculature in the vicinity of the electrode. Hemosiderin is also present in the vicinity of DBS electrodes, as reported recently in a postmortem study of a patient 71 months after implant [44]. The number of electrodes surrounded by hemosiderin-laden macrophages increased with time. The time course indicates that local hemorrhaging occurs not only from the acute injury, but at chronic time points as well. Vascular damage likely exacerbates the sustained activation of microglia next to the electrodes. Additionally, the effects of local ischemia at the electrode interface could be a cause of neurodegeneration. As mentioned previously, hemosiderin has been hypothesized as being a product of free radicals with ferritin [21], which suggests the local presence of reactive oxygen species (ROS) at the electrode. ROS are therefore a potential inflammatory mediator for the observed neurodegenerative features next to the electrode. Indeed, persistent thrombin signaling induces oxidative stress and has been shown to lead to tau hyperphosphorylation and delayed neuronal death [45, 46]. In

addition to ROS, the contribution of other pro-inflammatory mediators of inflammation, including cytokines and nitric oxide, should be considered as a mechanistic link(s) between chronic inflammation and local neurodegeneration in future studies.

We observed a significant increase in NeuN and MAP-2 positive signal, together with a decrease in Fluoro-Jade C, after 8 weeks compared to 2 weeks. One possible explanation is based on the development of the astrocytic scar surrounding the electrode. Astrocytes are more widely dispersed at 2 weeks, and become more compact after 8 weeks (compare figure 1(b3) with figure 1(c3)). As astrocyte becomes more tightly associated with the electrode at 8 weeks, more neurons and dendrites may have more space to move closer to the electrode compared to after 2 weeks. An alternative hypothesis is that the neurons regenerate from 2 weeks to 8 weeks and then degenerate from 8 weeks to 16 weeks. While this would be surprising, it is possible that the effects of cumulative neurotoxic inflammatory mediators caused by chronic inflammation (inducing degeneration) may overcome the effects of neurotrophic levels (for regeneration) only at longer time points than 8 weeks.

The results of this study suggest that chronic inflammation and associated local neurodegeneration may contribute to recording failure. Reducing inflammation through delivery of anti-inflammatory agents may be beneficial for chronic recordings, since the consequent neurodegeneration might also be slowed or halted. Experimental data suggest that target neurons for recordings must be within 100 μm [47]. We observed increased neuronal death, dendritic loss and tau pathology within this critical region. Further studies are needed to determine the functional consequences of these neurodegenerative features on target neurons.

5. Conclusion

In conclusion, we present evidence that provides a potential explanation for the temporal discrepancy between stabilization of astroglial scar's electrical properties and the typical time course of recording failures. This study demonstrates that the chronic presence of neural electrodes results in a persistent local inflammation, and that this local inflammation in turn correlates to the expression of markers associated with neurodegeneration. This finding is critical in two ways. First, it offers an alternate and perhaps more accurate explanation for the failure of chronically implanted neural electrodes. Second, it informs potential strategies to overcome recording failures. Therefore, these findings have important implications for chronically implanted electrodes, and the field of neuroprosthetics.

Acknowledgments

Funding support was provided by the NIH, R01 DC06849 (RVB) and NIH NS 045072 (RVB). GTEC, an NSF funded ERC located at Georgia Institute of Technology and Emory University (EEC-9731643), is also acknowledged for the use of core facilities.

References

- [1] Carmena J M, Lebedev M A, Crist R E, O'Doherty J E, Santucci D M, Dimitrov D F, Patil P G, Henriquez C S and Nicolelis M A 2003 Learning to control a brain-machine interface for reaching and grasping by primates *PLoS Biol.* **1** E42
- [2] Chapin J K, Moxon K A, Markowitz R S and Nicolelis M A 1999 Real-time control of a robot arm using simultaneously recorded neurons in the motor cortex *Nat. Neurosci.* **2** 664–70
- [3] Hochberg L R, Serruya M D, Friehs G M, Mukand J A, Saleh M, Caplan A H, Branner A, Chen D, Penn R D and Donoghue J P 2006 Neuronal ensemble control of prosthetic devices by a human with tetraplegia *Nature* **442** 164–71
- [4] Lebedev M A, Carmena J M, O'Doherty J E, Zacksenhouse M, Henriquez C S, Principe J C and Nicolelis M A 2005 Cortical ensemble adaptation to represent velocity of an artificial actuator controlled by a brain-machine interface *J. Neurosci.* **25** 4681–93
- [5] Serruya M D, Hatsopoulos N G, Paninski L, Fellows M R and Donoghue J P 2002 Instant neural control of a movement signal *Nature* **416** 141–2
- [6] Taylor D M, Tillery S I and Schwartz A B 2002 Direct cortical control of 3d neuroprosthetic devices *Science* **296** 1829–32
- [7] Wessberg J, Stambaugh C R, Kralik J D, Beck P D, Laubach M, Chapin J K, Kim J, Biggs S J, Srinivasan M A and Nicolelis M A 2000 Real-time prediction of hand trajectory by ensembles of cortical neurons in primates *Nature* **408** 361–5
- [8] Merrill D R and Tresco P A 2005 Impedance characterization of microarray recording electrodes *in vitro IEEE Trans. Biomed. Eng.* **52** 1960–5
- [9] Liu X, McCreery D B, Carter R R, Bullara L A, Yuen T G and Agnew W F 1999 Stability of the interface between neural tissue and chronically implanted intracortical microelectrodes *IEEE Trans. Rehabil. Eng.* **7** 315–26
- [10] Nicolelis M A, Dimitrov D, Carmena J M, Crist R, Lehw G, Kralik J D and Wise S P 2003 Chronic, multisite, multielectrode recordings in macaque monkeys *Proc. Natl Acad. Sci. USA* **100** 11041–6
- [11] Rousche P J and Normann R A 1998 Chronic recording capability of the Utah intracortical electrode array in cat sensory cortex *J. Neurosci. Methods* **82** 1–15
- [12] Williams J C, Rennaker R L and Kipke D R 1999 Long-term neural recording characteristics of wire microelectrode arrays implanted in cerebral cortex *Brain. Res. Brain Res. Protoc.* **4** 303–13
- [13] Biran R, Martin D C and Tresco P A 2005 Neuronal cell loss accompanies the brain tissue response to chronically implanted silicon microelectrode arrays *Exp. Neurol.* **195** 115–26
- [14] Biran R, Martin D C and Tresco P A 2007 The brain tissue response to implanted silicon microelectrode arrays is increased when the device is tethered to the skull *J. Biomed. Mater. Res. A* **82** 169–78
- [15] Vetter R J, Williams J C, Hetke J F, Nunamaker E A and Kipke D R 2004 Chronic neural recording using silicon-substrate microelectrode arrays implanted in cerebral cortex *IEEE Trans. Biomed. Eng.* **51** 896–904
- [16] Ludwig K A, Uram J D, Yang J, Martin D C and Kipke D R 2006 Chronic neural recordings using silicon microelectrode arrays electrochemically deposited with a poly(3,4-ethylenedioxythiophene) (PEDOT) film *J. Neural Eng.* **3** 59–70
- [17] McConnell G C, Schneider T M, Owens D J and Bellamkonda R V 2007 Extraction force and cortical tissue

- reaction of silicon microelectrode arrays implanted in the rat brain *IEEE Trans. Biomed. Eng.* **54** 1097–107
- [18] Schmued L C, Stowers C C, Scallet A C and Xu L 2005 Fluoro-jade c results in ultra high resolution and contrast labeling of degenerating neurons *Brain Res.* **1035** 24–31
- [19] Szarowski D H, Andersen M D, Retterer S, Spence A J, Isaacson M, Craighead H G, Turner J N and Shain W 2003 Brain responses to micro-machined silicon devices *Brain Res.* **983** 23–35
- [20] Turner J N, Shain W, Szarowski D H, Andersen M, Martins S, Isaacson M and Craighead H 1999 Cerebral astrocyte response to micromachined silicon implants *Exp. Neurol.* **156** 33–49
- [21] O'Connell M J, Baum H and Peters T J 1986 Haemosiderin-like properties of free-radical-modified ferritin *Biochem. J.* **240** 297–300
- [22] Block M L and Hong J S 2005 Microglia and inflammation-mediated neurodegeneration: multiple triggers with a common mechanism *Prog. Neurobiol.* **76** 77–98
- [23] Block M L, Zecca L and Hong J S 2007 Microglia-mediated neurotoxicity: uncovering the molecular mechanisms *Nat. Rev. Neurosci.* **8** 57–69
- [24] Lee V M, Goedert M and Trojanowski J Q 2001 Neurodegenerative tauopathies *Ann. Rev. Neurosci.* **24** 1121–59
- [25] Edell D J, Toi V V, McNeil V M and Clark L D 1992 Factors influencing the biocompatibility of insertable silicon microshafts in cerebral cortex *IEEE Trans. Biomed. Eng.* **39** 635–43
- [26] Castillo-Ruiz M M, Campuzano O, Acarin L, Castellano B and Gonzalez B 2007 Delayed neurodegeneration and early astrogliosis after excitotoxicity to the aged brain *Exp. Gerontol.* **42** 343–54
- [27] Collombet J M, Masqueliez C, Four E, Burckhart M F, Bernabe D, Baubichon D and Lallement G 2006 Early reduction of neuron antigenicity induced by soman poisoning in mice can be used to predict delayed neuronal degeneration in the hippocampus *Neurosci. Lett.* **398** 337–42
- [28] Eisch A J and Marshall J F 1998 Methamphetamine neurotoxicity: dissociation of striatal dopamine terminal damage from parietal cortical cell body injury *Synapse* **30** 433–45
- [29] Hellmich H L, Eidson K A, Capra B A, Garcia J M, Boone D R, Hawkins B E, Uchida T, Dewitt D S and Prough D S 2007 Injured fluoro-jade-positive hippocampal neurons contain high levels of zinc after traumatic brain injury *Brain Res.* **1127** 119–26
- [30] Jicha G A, Lane E, Vincent I, Otvos J, Hoffmann L R and Davies P 1997 A conformation- and phosphorylation-dependent antibody recognizing the paired helical filaments of Alzheimer's disease *J. Neurochem.* **69** 2087–95
- [31] Augustinack J C, Schneider A, Mandelkow E M and Hyman B T 2002 Specific tau phosphorylation sites correlate with severity of neuronal cytopathology in Alzheimer's disease *Acta Neuropathol. (Berl.)* **103** 26–35
- [32] Luna-Munoz J, Garcia-Sierra F, Falcon V, Menendez I, Chavez-Macias L and Mena R 2005 Regional conformational change involving phosphorylation of tau protein at the thr231, precedes the structural change detected by alz-50 antibody in Alzheimer's disease *J. Alzheimers Dis.* **8** 29–41
- [33] Weaver C L, Espinoza M, Kress Y and Davies P 2000 Conformational change as one of the earliest alterations of tau in Alzheimer's disease *Neurobiol. Aging* **21** 719–27
- [34] Cho J H and Johnson G V 2004 Primed phosphorylation of tau at thr231 by glycogen synthase kinase 3beta (gsk3beta) plays a critical role in regulating tau's ability to bind and stabilize microtubules *J. Neurochem.* **88** 349–58
- [35] Lin G, Chawla M K, Olson K, Barnes C A, Guzowski J F, Bjornsson C, Shain W and Roysam B 2007 A multi-model approach to simultaneous segmentation and classification of heterogeneous populations of cell nuclei in 3d confocal microscope images *Cytometry A* **71** 724–36
- [36] Alonso A, Zaidi T, Novak M, Grundke-Iqbal I and Iqbal K 2001 Hyperphosphorylation induces self-assembly of tau into tangles of paired helical filaments/straight filaments *Proc. Natl Acad. Sci. USA* **98** 6923–8
- [37] Vincent I, Zheng J H, Dickson D W, Kress Y and Davies P 1998 Mitotic phosphoepitopes precede paired helical filaments in Alzheimer's disease *Neurobiol. Aging* **19** 287–96
- [38] Liu B and Hong J S 2003 Role of microglia in inflammation-mediated neurodegenerative diseases: mechanisms and strategies for therapeutic intervention *J. Pharmacol. Exp. Ther.* **304** 1–7
- [39] Qin L, Wu X, Block M L, Liu Y, Breese G R, Hong J S, Knapp D J and Crews F T 2007 Systemic lps causes chronic neuroinflammation and progressive neurodegeneration *Glia* **55** 453–62
- [40] Dias-Santagata D, Fulga T A, Duttaray A and Feany M B 2007 Oxidative stress mediates tau-induced neurodegeneration in drosophila *J. Clin. Invest.* **117** 236–45
- [41] Melov S *et al* 2007 Mitochondrial oxidative stress causes hyperphosphorylation of tau *PLoS ONE* **2** e536
- [42] Kitazawa M, Oddo S, Yamasaki T R, Green K N and LaFerla F M 2005 Lipopolysaccharide-induced inflammation exacerbates tau pathology by a cyclin-dependent kinase 5-mediated pathway in a transgenic model of Alzheimer's disease *J. Neurosci.* **25** 8843–53
- [43] Yoshiyama Y, Higuchi M, Zhang B, Huang S M, Iwata N, Saito T C, Maeda J, Suhara T, Trojanowski J Q and Lee V M 2007 Synapse loss and microglial activation precede tangles in a p301s tauopathy mouse model *Neuron* **53** 337–51
- [44] Sun D A, Yu H, Spooner J, Tatsas A D, Davis T, Abel T W, Kao C and Konrad P E 2008 Postmortem analysis following 71 months of deep brain stimulation of the subthalamic nucleus for Parkinson disease *J. Neurosurg.* **109** 325–9
- [45] Suo Z, Wu M, Citron B A, Palazzo R E and Festoff B W 2003 Rapid tau aggregation and delayed hippocampal neuronal death induced by persistent thrombin signaling *J. Biol. Chem.* **278** 37681–9
- [46] Choi S H, Lee D Y, Kim S U and Jin B K 2005 Thrombin-induced oxidative stress contributes to the death of hippocampal neurons *in vivo*: role of microglial nadph oxidase *J. Neurosci.* **25** 4082–90
- [47] Henze D A, Borhegyi Z, Csicsvari J, Mamiya A, Harris K D and Buzsaki G 2000 Intracellular features predicted by extracellular recordings in the hippocampus *in vivo* *J. Neurophysiol.* **84** 390–400